

POLARIZATION LIDAR USING A LIQUID CRYSTAL VARIABLE RETARDER

Joseph A. Shaw, Nathan L. Seldomridge, Kevin S. Repasky

Electrical and Computer Engineering Department, Montana State University, Bozeman, MT USA 59717
jshaw@montana.edu

ABSTRACT

We describe a dual-polarization lidar that uses a liquid crystal variable retarder to switch the receiver polarization state on alternate laser shots with pulse repetition frequency up to 30 Hz. Depolarization ratios at 532 nm can be measured with an additive error within 0.4% for the entire system (including the liquid crystal and a Schmidt-Cassegrain receiver telescope). The lidar is designed for upward-looking measurements of clouds and aerosols with a narrow field of view or downward-looking airborne measurements of the terrestrial and marine environment with a field of view up to 8.8 mrad. Sample data are shown for clouds and a thin depolarizing layer of possibly Asian dust measured over Bozeman, Montana in March 2005.

1. INTRODUCTION

Polarization lidars are used in measurements that include aerosols and clouds, vegetation, soils, fish, and insects [1,2]. These lidar systems generally use either a single detector with time-sequential polarization switching, or multiple detectors with simultaneous polarization switching. The time-sequential approach benefits from fewer components and single-detector calibration, while the multiple-detector approach benefits from simultaneous polarization measurements but requires more receiver components.

This paper describes a lidar that has been developed for dual-polarization measurements in a wide range of ground-based and airborne applications. The 532-nm Nd:Yag transmitter (118-mJ pulse energy) is linearly polarized and the receiver uses a single photomultiplier tube detector with a liquid crystal variable retarder (LCVR) that provides electronic control of the receiver polarization state. The LCVR can switch just fast enough to provide shot-to-shot measurements of co-polarized and cross-polarized signals with the laser's 30-Hz maximum pulse repetition frequency (PRF). This technique could be employed on a lidar with a faster PRF by switching polarization states between groups of shots rather than alternate shots. The alternate-shot method has been implemented previously on a fast-pulse lidar with a Pockels cell [3], but Pockels cells require high switching voltages and limit the field of view with small apertures and long lengths. Conversely, the LCVR in our system uses switching voltages less than 5V and has a 40-mm-diameter clear aperture.

Several of the issues we explored in characterizing this system were the variation of LCVR behavior with temperature and incidence angle and the depolarizing effect of the reflective telescope. With reasonable temperature control of the LCVR, the lidar measures the depolarization ratio with an additive error that is within 0.4%, even at the full field of view allowed by the telescope (≤ 8.8 mrad). We demonstrate the use of this lidar in measuring clouds and a depolarizing layer near 8 km altitude over Bozeman, Montana in March 2005.

2. INSTRUMENT DESCRIPTION

Fig. 1 shows a schematic diagram of the lidar. The 532-nm laser pulses at 30-Hz PRF are detected by a photodiode near the laser to trigger the delay generator that controls the lidar timing. The transmitter beam is steered with two plane mirrors to facilitate alignment.

The receiver employs a Schmidt-Cassegrain reflective telescope with a 20.3-cm (diameter) primary aperture and a 6.9-cm secondary mirror central obscuration. The telescope directs received light through a field stop, interference filter (1 nm bandwidth centered at 532 nm), field lens, LCVR, and a fixed-angle linear polarizer, all contained in a light-tight box. The field-stop size can be changed to vary the receiver field of view up to 8.8 mrad. The interference filter is placed in the optical space with the shallowest ray angles ($< 2.8^\circ$ at the 8.8-mrad maximum field of view) to minimize angular tuning of the filter bandwidth.

At the output of the optics box is a gated photomultiplier tube (PMT) detector whose output is sampled at 100 MHz with 14 bits by an analog-to-digital (A/D) converter in a standard personal computer. The 10-ns laser pulse duration and the A/D sample rate of 100 MS/s both limit the range resolution to 1.5 m. The optics package is relatively compact, consisting of a 30.5 cm \times 91.5 cm aluminum plate with the transmitter on one side and receiver on the other.

At the widest field-of-view setting, the transmitter and receiver beams are in full overlap at altitudes between 80 m and beyond 15 km, where we end data acquisition (the minimum range for data acquisition is 10 m, determined by delays in the electronics). For the current biaxial configuration with a raw, unexpanded laser beam, the minimum overlap altitude moves upward for

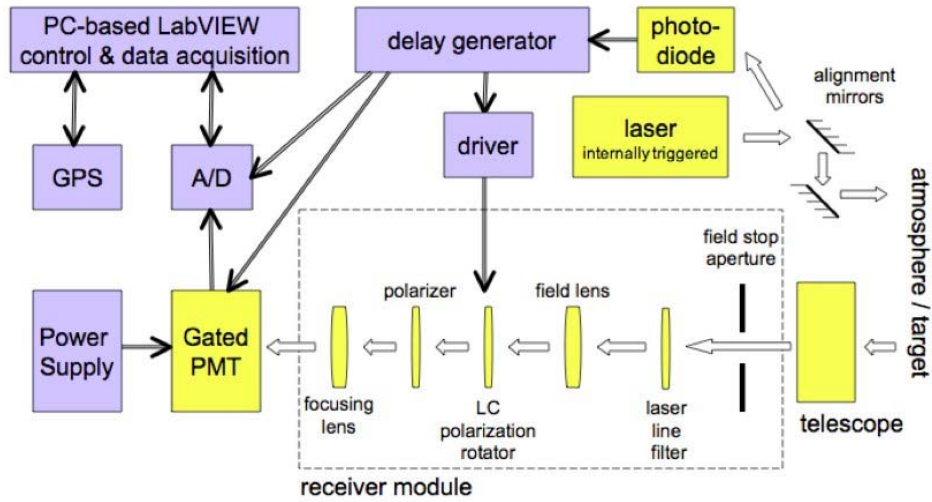


Fig. 1 Schematic diagram of the dual-polarization lidar using a liquid crystal (LC) variable retarder to switch receiver polarization states between 30-Hz laser pulses.

narrower receiver fields of view. Overlap calculations [1] show that the minimum altitude for 99.9% overlap is 80 m at 8.8 mrad field of view and rises to 500 m at 4.4 mrad. A very small field of view (≤ 1 mrad), which is necessary to minimize the effects of multiple scattering, will be made more practical with future modifications that include expansion of the transmitted laser beam.

We use a Meadowlark Optics temperature-controlled nematic LCVR with the slow axis oriented 45° from the transmitted polarization. The LCVR is followed by a Meadowlark film polarizer (extinction better than $10^5:1$), oriented parallel to the transmitted polarization. With the LCVR temperature stabilized at 40°C , the LCVR is maintained in the zero-retardance state (co-pol) with a zero-mean 2-kHz voltage square wave of amplitude ± 4.950 V and at the $\lambda/2$ state (cross-pol) with a zero-mean 2-kHz voltage square wave with amplitude ± 2.055 V. The square-wave amplitude is switched in the time between laser pulses, with LCVR switching times of 22 ms to go from zero to $\lambda/2$ retardance and 9 ms to go from $\lambda/2$ to zero retardance. This is fast enough to allow switching between 30 Hz laser pulses if the device is switched soon after the laser pulse. Although this is significantly slower than the switching speeds of Pockels cells, the LCVR uses much lower voltages that have insignificant switching noise.

Both the retardance and effective angle of rotation of a liquid crystal depend on incidence angle. For the widest field of view, the ray angle in this region of the receiver is less than 5° . Xiao et al. [4] showed that for similar conditions (a liquid crystal oriented at 45° and set near a $\lambda/2$ retardance), external incidence angles of 5° cause the retardance to vary by about 0.08λ and the 45° rotation angle to vary by about 2° . With both of these

errors maximized, the resulting Mueller matrix predicts a worst-case depolarization-ratio error of 2.0% for rays incident at 5° . However, only a small fraction of the light has a 5° incidence angle, so no measurement will have a full 2% error (but this does make smaller field angles preferable). The sample data presented in this paper were all taken with the maximum field of view (8.8 mrad) to confirm that the LCVR technique works sufficiently well at this setting.

3. POLARIZATION ACCURACY

We measured the polarization accuracy of the system with a variety of techniques described in more detail elsewhere [1,2]. The laser transmitter beam was found to be linearly polarized to within 7.5×10^{-4} (1,333:1).

A continuous-wave Nd:Yag 532-nm laser was used with a Glan-laser polarizer to provide a test beam with $10^5:1$ polarization purity and a film polarizer with extinction $7 \times 10^4:1$ was used as an analyzer. This test beam and analyzer were used to determine that the entire receiver provides a worst-case polarization error of 0.0038 (0.38%) when the receiver is illuminated with perfectly co-polarized light. The telescope alone was found to have negligible depolarization for fields of view up to 8.8 mrad. At 8.8 mrad the telescope depolarization measurements with three different techniques varied from 1.5×10^{-5} (66,667:1) to 4.7×10^{-4} (2,137:1).

We used the test beam and analyzer described previously to measure the transmittance of the full receiver (telescope, LCVR, polarizer, filters, and lenses). These transmittances were made at the LCVR zero- and half-wave retardance settings, with the receiver illuminated with a co-polarized (co-pol) and cross-polarized (x-pol) test beam (see Table 1).

Table 1: Measured transmittance of the entire receiver (with the liquid crystal set at zero and $\lambda/2$ retardances) for co-pol and cross-pol incident light (made with a laser line filter with transmittance = 0.5212).

	Liquid Crystal Setting		
	<i>zero retardance</i> (4.950 V)	<i>half-wave retardance</i> (2.055 V)	<i>without LCVR</i>
<i>Co-pol</i>	$T_{0\parallel} = 0.3653$	$T_{\frac{\lambda}{2}\parallel} = 0.0014$	$T_{\parallel} = 0.3993$
<i>x-pol</i>	$T_{0\perp} = 0.0019$	$T_{\frac{\lambda}{2}\perp} = 0.3651$	$T_{\perp} = 0.0002$

4. SAMPLE DATA

In this section we show sample data, taken with the lidar pointed at the zenith sky through a laboratory roof port. We used the widest field-of-view setting to carefully test the receiver (a narrower field of view would be needed to reduce multiple scattering in cloud lidar studies). One data file was saved each minute, and passed through a shot-to-shot 3-point median filter to reduce noise and occasional LCVR switching errors. To compensate for the partially polarized sky light in the two channels, different sky background levels were subtracted from the co-pol and cross-pol signals. The offset for each shot is the median of the samples in the altitude range of 14-15 km (a procedure which effectively removes the molecular scattering signal). The data were range corrected and the depolarization ratio computed from each pair of laser shots.

Figs 2 and 3 show vertical profiles of the backscattered co-pol signal and depolarization ratio, respectively, for a low-depolarizing layer at 4.2 km and a highly depolarizing layer at 7.8 km (3 Mar., 2005, 04:19 UTC) over Bozeman, Montana (45.67 °N, 111.05 °W). The lower layer, for which the air temperature was measured by a radiosonde to be -25 °C, has a depolarization ratio of 0.023, which is typical of super-cooled liquid clouds. Above this liquid layer is another thin layer with temperature well below -40 °C (the radiosonde launch terminated early). This higher layer could be either ice or an elevated aerosol layer. Two additional layers can be seen at 8.4 and 8.6 km, both with depolarization ~ 0.1 from very faint signals.

The elevated scattering layers near 8 km persisted for several days from our first detection on 1 Mar., 2005, shown in Figs. 4 and 5 (1 March, 2005, 03:32 UTC). These figures show at least four distinguishable depolarizing layers between 6.9 and 8.7 km. All these layers were subvisual, with stars clearly visible through them. The air temperature at these altitudes ranged from -47 to -60 °C, and the depolarization ratio ranged from

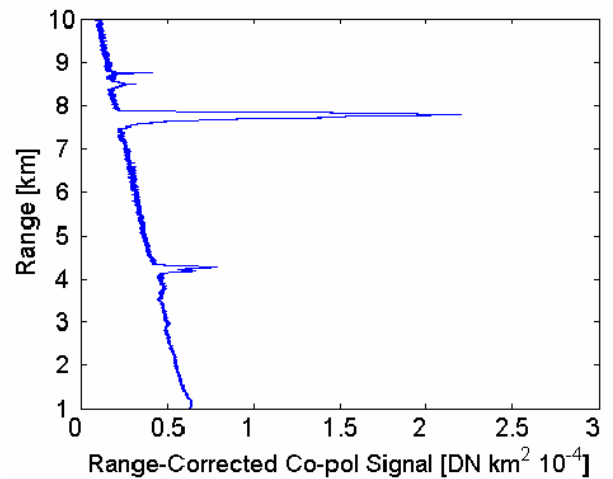


Fig. 2. Vertical profile of range-corrected co-polarized backscatter signal (3 March, 2005, 0419 UTC).

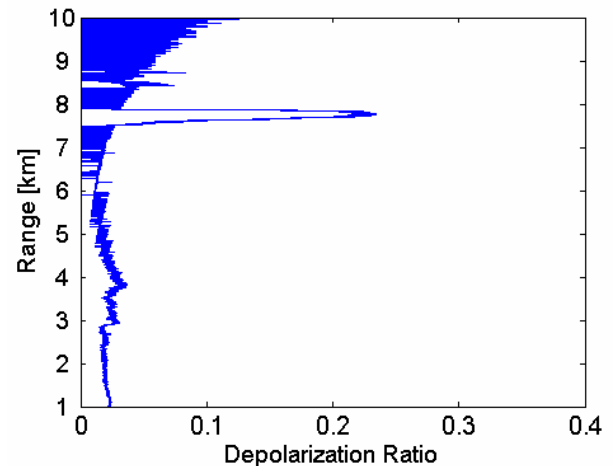


Fig. 3. Vertical profile of depolarization ratio corresponding to the backscatter profile in Fig. 2.

0.18 to 0.25. The air temperature and depolarization measurements suggest that these layers are either subvisual cirrus or aerosols, or some combination thereof. Our radiosonde data show the relative humidity over ice to be less than 40% below 8km and near 100% between 8 and 9 km. Therefore, the depolarizing layers above 8 km could be subvisual cirrus, but this does not necessarily explain the layers at lower altitudes ($\sim 7-8$ km). An alternate explanation for at least some of the high, thin, depolarizing layers observed consistently over the period 1-3 March is elevated aerosol layers or a combination of aerosols and thin cirrus clouds nucleated by the dust [5].

We hypothesize that the elevated scattering layers measured on 1-3 Mar., 2005 over Bozeman, Montana was Asian dust, or possibly Asian dust mixed with subvisual cirrus that may have been nucleated by the

dust [5]. A back-trajectory analysis was performed with the NOAA HYSPLIT model [6] using defaults for the vertical transport model. This analysis shows that air from 7500 m AGL over Bozeman came from 3500 m over east-central China ten days earlier (passing over ocean for 6-7 days and western Canada for 3 days (with very low convective potential energy and no fires).

Around 20 February 2005, there was thick haze over Beijing and most of central China, but the air was very stable, so the likelihood is low that haze could have risen out of the boundary layer to an altitude where it would be blown eastward. It is more likely that sand on

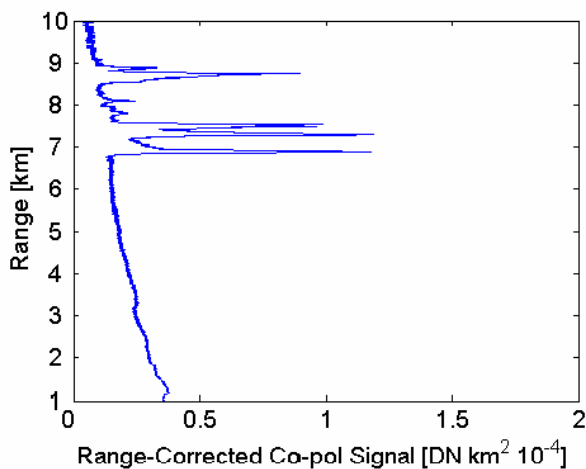


Fig. 4. Vertical profile of range-corrected co-polarized backscatter (1 Mar, 2005, 03:32 UTC).

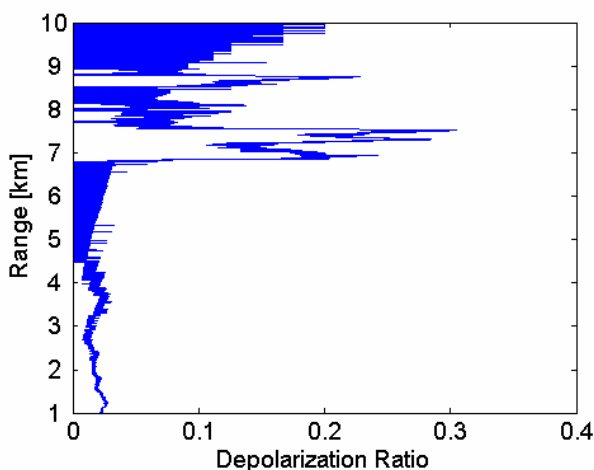


Fig. 5. Vertical profile of depolarization ratio corresponding to backscatter profile in Fig. 4.

the Tibetan plateau, at an elevation of about 3500 m, was blown across this stable air and out over the Pacific [7,8] (rawinsonde data indicate strong westerly winds over the Tibetan plateau and across central China during this time period). Given all the available information, Asian dust mixed with subvisual cirrus appears to be a reasonable explanation of these observations.

ACKNOWLEDGMENT

We gratefully acknowledge financial support from the NASA Ames Research Center and from the NASA Graduate Student Research Program via the Stennis Space Center. We express appreciation to the NOAA Air Resources Laboratory for providing the HYSPLIT transport and dispersion model used in the analysis reported in this paper.

REFERENCES

1. N. L. Seldomridge, *Dual-polarization cloud lidar design and characterization*, M.S. Thesis, Montana State Univ., Bozeman, MT, 2005 (www.montana.edu/etd/available/seldomridge_0805.html).
2. N. L. Seldomridge, J. A. Shaw, and K. S. Repasky, Dual-polarization lidar using a liquid crystal variable retarder, *Opt. Eng.* (in press), 2006.
3. J. M. Intrieri, M. D. Shupe, T. Uttal, and B. J. McCarty, An annual cycle of Arctic cloud characteristics observed by radar and lidar at SHEBA, *J. Geophys. Res.* Vol. 107, SHE5-1-15, 2002.
4. X. Xiao, D. Voelz, and H. Sugiura, Field of view characteristics of a liquid crystal variable retarder, *Proc. SPIE* Vol. 5158, 142-150, 2003.
5. K. Sassen, Dusty ice clouds over Alaska, *Nature* Vol. 434, 456, 2005.
6. R. R. Draxler and G. D. Rolph, HYSPLIT (HYbrid Single-Particle Lagrangian Integrated Trajectory) model access via NOAA ARL READY website (<http://www.arl.noaa.gov/ready/hysplit4.html>). NOAA Air Resources Laboratory, Silver Spring, MD, 2003.
7. S. A. Bowling and G. E. Shaw, The thermodynamics of pollutant removal as an indicator of possible source areas for Arctic haze, *Atmos. Environ.* Vol. 26A(16), 2953-2961, 1992.
8. G. E. Shaw, personal communication, Geophysical Institute, University of Alaska, Fairbanks, AK, 99775, gshaw@gi.alaska.edu, 2005.